





ORIGINAL ARTICLE

Bleb morphology of glaucoma drainage devices on magnetic resonance imaging

Rafael Correia Barão^{1,2}  | David Berhanu^{3,4}  | Diogo Bernardo Matos^{1,2}  |
 André Diogo Barata^{1,2}  | Rita Sousa³  | Luís Abegão Pinto^{1,2} 

¹Department of Ophthalmology, Hospital de Santa Maria, CHULN, Lisbon, Portugal

²Visual Sciences Study Center, Faculty of Medicine, University of Lisbon, Lisbon, Portugal

³Department of Neurological Imaging, Hospital de Santa Maria, CHULN, Lisbon, Portugal

⁴Anatomy Institute, Faculty of Medicine, University of Lisbon, Lisbon, Portugal

Correspondence

Rafael Correia Barão, Departamento de Oftalmologia, Hospital de Santa Maria, Av. Prof. Egas Moniz, 1649-035 Lisboa, Portugal.

Email: rafaelcbarao@gmail.com

Abstract

Purpose: To evaluate bleb morphology features of different glaucoma drainage devices (GDD) using magnetic resonance imaging (MRI).

Materials and Methods: Prospective cohort study of GDD and bleb morphology in consecutive glaucoma patients implanted with Ahmed Glaucoma Valve (AGV), Paul Glaucoma Implant (PGI), Baerveldt Glaucoma Implant (BGI) and Ahmed ClearPath (ACP) devices. Thirty-six eyes from 30 consecutive patients underwent standardized GDD implantation followed by MRI at least 1 month after surgery. Main outcomes included bleb volume and endplate position relative to the optic nerve. Secondary outcomes included intraocular pressure (IOP), medication and surgical complications during a 12-month follow-up.

Results: Seven eyes were implanted with the AGV (19%), 5 with BGI (14%), 16 with PGI (44%) and 8 with ACP (22%). MRI scans were obtained 85 ± 66 days after surgery. Mean total bleb volume was $563 \pm 390 \text{ mm}^3$. This bleb volume was inversely correlated with early post-operative IOP (day 7; $r_s = -0.3326$, $p = 0.0475$) but positively correlated with IOP at 12 months ($r_s = 0.3592$, $p = 0.0341$). No significant difference in total bleb volume was found between GDD types ($p = 0.1223$). A double-layered bleb was observed in 34 eyes (94%). The inferior bleb volume was significantly larger in PGI devices versus other GDD types (380 ± 205 vs. $193 \pm 161 \text{ mm}^3$; $p = 0.0043$). Distance from the endplate to the optic nerve was $9.5 \pm 4.0 \text{ mm}$, similar across GDDs ($p = 0.2519$).

Conclusions: Double-layered blebs are a common finding with GDDs. Bleb volume showed different correlations with IOP at distinct timepoints and the PGI device formed larger blebs. A standardized GDD implantation technique ensures a safe distance from the GDD endplate to the optic nerve.

KEYWORDS

aqueous shunt, glaucoma, glaucoma surgery, long tube, magnetic resonance imaging, orbit

1 | INTRODUCTION

The spectrum of surgical options for glaucoma has widened in recent years (Conlon et al., 2017; Yang et al., 2021). The use of glaucoma drainage devices (GDDs) in the management of medically uncontrolled glaucoma increased and is now common across glaucoma surgeons (Desai et al., 2011; Rathi et al., 2021; Vinod et al., 2017; Yang et al., 2021). Two glaucoma drainage devices have been extensively studied: the Ahmed Glaucoma Valve FP7 (AGV) and the

Baerveldt Glaucoma Implant (BGI) (Barton et al., 2011; Budenz et al., 2015, 2016; Christakis et al., 2016; Tsai & Budenz, 2017). Recently, two GDDs have been introduced in clinical practice, the Paul Glaucoma Implant (PGI) and Ahmed ClearPath (ACP) with early positive results (Dorairaj et al., 2022; Grover et al., 2022; José et al., 2022; Koh et al., 2020; Tan et al., 2022; Vallabh et al., 2022).

All these GDDs share common design features to provide sustained aqueous humour (AH) outflow. A hollow flexible tube drains AH from the anterior chamber

This is an open access article under the terms of the [Creative Commons Attribution-NonCommercial](https://creativecommons.org/licenses/by-nc/4.0/) License, which permits use, distribution and reproduction in any medium, provided the original work is properly cited and is not used for commercial purposes.

© 2023 The Authors. *Acta Ophthalmologica* published by John Wiley & Sons Ltd on behalf of Acta Ophthalmologica Scandinavica Foundation.

(AC) to the subconjunctival space for absorption (Siggel et al., 2020; Yu et al., 2009). The external end of the tube connects to a fenestrated endplate implanted in the subconjunctival space acting as a reservoir and/or a spacer, allowing the AH to be spread across a large surface area, thereby creating a filtering bleb (Minckler et al., 1987). Bleb morphology assessments, such as bleb height, width and thickness, play an important role in defining a 'healthy' filtering bleb after glaucoma surgery (Hoffmann et al., 2020; Khamar et al., 2014; Oh et al., 2017; Waibel et al., 2019). However, these features are difficult to directly assess at the slit-lamp in eyes implanted with a GDD because the filtering bleb is more posterior in the orbital cavity. Although previous publications have reported some clinical correlations of AGV and BGI bleb parameters using different imaging modalities, the role of endplate design, surface area, tube size and bleb morphology in successful GDD surgery is still unclear (Detorakis et al., 2009; Ferreira et al., 2015; Iwasaki et al., 2017; Jung et al., 2015; Sano et al., 2015; Wagdy, 2020).

The purpose of this study is to analyse magnetic resonance imaging bleb morphology features and endplate position with different types of GDD and explore clinical correlations.

2 | MATERIALS AND METHODS

2.1 | Study design and population

Prospective observational study undertaken at Hospital Santa Maria, CHULN, Lisbon, Portugal, from 2019 to 2022, approved by the CHULN Ethics Committee (approval ref. 489/19). Inclusion criteria included adult patients with medically uncontrolled glaucoma who needed implantation of a GDD. Patients unwilling or with contraindications to undergo MRI were not included. All patients signed consent forms and this study follow the tenets of the Declaration of Helsinki.

2.2 | Glaucoma drainage devices

Four different types of GDD were implanted: AGV FP7 model (New World Medical), BGI 350 mm² (Advanced Medical Optics), PGI (Advanced Ophthalmic

Innovations) and ACP 350 mm² (New World Medical). Features of these GDD are summarized in Table 1.

2.3 | Surgical technique

Glaucoma drainage devices (GDD) implantation technique was performed as follows: the endplate was implanted in a supero-temporal sub-Tenon's pocket after performing a fornix-based peritomy and conjunctiva and Tenon's layer blunt dissection. The endplate was secured to the sclera with 8-0 nylon sutures 10 mm from the limbus. The endplate wings of the BGI, PGI and ACP devices were tucked under the superior and lateral recti muscles. A 3-0 polypropylene suture was passed into the BGI tube as a hypotony prevention measure (pre-placed in the ACP). No ab luminal stent was placed in the PGI or the AGV. The AGV valve system was primed with balanced-salt solution through a 30-gauge needle before implantation.

Sponges soaked with 0.4 mg/dL mitomycin C (MMC) were placed for 90 s over the endplate. A needle tract (23-gauge for the AGV, BGI, ACP; 25-gauge for the BGI) was initiated 3 mm from the limbus, upon which the tube was trimmed bevel-up and inserted into the AC. For BGI, PGI and ACP devices a single 7-0 polyglactin ligature was tied around the tube near its connection to the endplate, whereas an additional ligature was tightly placed near the scleral entry site of the PGI tube. The external length of the tube was secured to the sclera and covered with donor cornea tissue or a commercially available pericardium patch (Tutopatch®, Tutogen Medical GmbH), followed by conjunctival closure. Patients were instructed to stop all glaucoma medication and were started on antibiotic and dexamethasone drops 4 times daily for 2 weeks, tapered over 4–6 weeks.

2.4 | Ophthalmological examinations

All patients were examined pre-operatively at least 2 weeks before surgery. After the procedure patients were seen on days 1, 7, 14, months 1, 3, 6 and 12, and also on the day MRI was performed. Examinations included best-corrected visual acuity using Snellen charts (except on day 1), Goldmann applanation tonometry (GAT)

TABLE 1 Summary of main features of the four GDD used.

	Ahmed glaucoma valve FP7	Baerveldt glaucoma implant 350	Paul glaucoma implant	Ahmed ClearPath 350
Endplate surface area (mm ²)	184	350	342	350
Endplate length (mm)	16	15	16.1	16.48
Endplate width (mm)	13	32	21.9	30.47
Endplate thickness (mm)	1.0	0.84	0.95	0.86
Tube outer diameter (µm)	630	630	467	635
Tube inner diameter (µm)	300	300	127	305
Valved system	Yes	No	No	No
Endplate material	Medical grade silicone	Barium-impregnated medical grade silicone	Medical grade silicone	Barium-impregnated medical grade silicone

intraocular pressure (IOP) measurement, slit-lamp biomicroscopy and fundus examination.

2.5 | Magnetic resonance imaging (MRI)

All patients underwent orbital MRI at least 1-month after surgery to allow for conjunctival scarring and initial capsule formation (Ishida et al., 2021; Lloyd et al., 1996). Scans were performed in a 3-Tesla MRI scanner (Philips Achieva, Philips Medical Systems), using an 8-channel head coil. The imaging protocol included axial T1- and T2-weighted images with 2 mm thickness and a volumetric 3D T2-weighted sequence, with 1 mm thickness reconstructions in the axial, coronal and sagittal planes. Image analysis was executed with PACS (Sectra Workstation IDS7, Sweden) to perform bleb and endplate measurements. GDD endplates were identified as a dark hypointense structure in T1- and T2-weighted images adjacent to the eye. The surrounding filtering bleb was identified as a high-intensity structure on T2-weighted images. Bleb and globe volume measurements were taken using multiplanar and three-dimensional reconstructions by applying a bleb signal threshold in each cut. The minimum distance between the endplate anterior edge to the corneal limbus was measured in axial images where the endplate was seen most anteriorly, with a straight line from the endplate edge to the corneal limbus. The minimum distance between the posterior edge of the endplate to the optic nerve was measured similarly. All scans were analysed by a neurological imaging expert.

2.6 | Outcomes

Main outcome measures included bleb morphology and endplate position measurements, namely bleb volume, minimum distance between endplate to corneal limbus and optic nerve, and the presence of bleb under recti muscles. Other radiological and clinical variables recorded included axial length, globe volume, pre- and post-operative IOP measurements, number of medications and post-operative complications at all timepoints. Secondary outcomes included surgical success defined as 12-month post-operative IOP ≤ 18 and at least 20% reduction in IOP from baseline, with or without medications (qualified and absolute success). Surgical failure was defined as loss of ≥ 2 Snellen lines on two consecutive visits, sight-threatening complications or uncontrolled IOP needing surgical revision or another glaucoma procedure. The timepoint of surgical failure due to uncontrolled IOP was the first of two consecutive visits in which the above criteria were not met.

2.7 | Statistical analysis

Statistical analysis was performed with GraphPad Prism 9 (version 9.5.0). Kolmogorov–Smirnov and Shapiro–Wilk tests were used to assess distribution normality. Chi-square test was used to compare categorical variables and proportions. Student-*t* and Kolmogorov–Smirnov

tests were used for parametric and non-parametric quantitative data analysis, respectively. For comparisons between multiple variables ANOVA and Kruskal–Wallis tests were performed as appropriate. Linear correlation was assessed with Pearson and Spearman coefficients as appropriate. Kaplan–Meier survival curves were used to assess cumulative success probability for both absolute and qualified success at 12 months. Survival analysis included Mantel–Cox log rank test to compare probability of success. Cox proportional hazards regression was performed to assess risk factors for survival. A *p*-value < 0.05 was used to assert statistical significance.

3 | RESULTS

3.1 | Sample population

Thirty-six (36) eyes of 30 consecutive patients implanted with a GDD were included. Seven eyes were implanted with an AGV (19%), 5 with the BGI (14%), 16 with the PGI (44%) and 8 with the ACP device (22%). There was no significant difference between groups regarding age, sex, glaucoma diagnosis, previous surgeries, baseline IOP or medication. Patient demographic and clinical information is summarized in Table 2.

3.2 | Bleb morphology assessment

All patients underwent orbital imaging 85 ± 66 days after surgery, with no significant difference between GDDs ($p = 0.7052$). A double-bleb configuration was seen in 94% of eyes ($n = 34$; Figure 1). The two patients who did not present with a double-bleb configuration had been implanted with a BGI device and had their stents removed at month 1, days before undergoing MRI, with subsequent self-limited hypotony. Mean total bleb volume was $563 \pm 390 \text{ mm}^3$, with no significant difference across GDDs ($p = 0.1223$). Sub-analysis comparing PGI with the remaining devices shows larger blebs in the PGI subgroup (734 ± 434 vs. $427 \pm 286 \text{ mm}^3$; $p = 0.0167$). Mean inferior bleb volume was significantly different across GDD groups (mean volume of $276 \pm 202 \text{ mm}^3$; $p = 0.0108$), with smaller volumes seen with the AGV ($101 \pm 64 \text{ mm}^3$) and larger volumes with the PGI ($380 \pm 205 \text{ mm}^3$).

Twenty-two (22) eyes (61%) showed extension of the bleb under one or both adjacent recti muscles (Figure 2). This sign was visible in 3 BGI eyes (60% of that group), 13 PGI (81%) and 6 ACP (75%) and in no case implanted with an AGV ($p = 0.0024$). Scleral flattening under the endplate (Figure 1) was identified in 12 eyes (33%), mostly in PGI patients ($n = 10$; 63% of PGI eyes; $p = 0.0089$). This finding was closely associated with total bleb volume, being observed in 78% of blebs in volume quartile 75–100th ($p = 0.0049$) and absent in all eyes with blebs in quartile 0–25th ($p = 0.0334$). The minimum distance from the endplate to the limbus was $8.5 \pm 1.9 \text{ mm}$, similar in all groups ($p = 0.2301$), as was the distance to the optic nerve ($9.5 \pm 4.0 \text{ mm}$; $p = 0.2519$). Radiological findings are detailed in Table 3.

TABLE 2 Summary of sample demographics, clinical information and surgical outcomes.

	Total	AGV	BGI	PGI	ACP	<i>p</i> -value
Eyes, <i>N</i>	36	7	5	16	8	0.0157 ^b
Patients, <i>N</i> ^a	30	7	5	13	8	0.1212 ^b
Age (m±SD)	57.1±20	67.4±9.3	56±24	50.7±21	61.5±19	0.2678 ^c
Female: male ratio	17:9	5:2	3:2	9:4	2:6	0.1902 ^b
Glaucoma diagnosis, <i>N</i> (% of eyes)						
POAG	6 (17)	1	2	3	0	0.3032 ^b
PACG	4 (11)	0	1	1	2	0.3589 ^b
SOAG	6 (17)	0	1	2	3	0.2467 ^b
SACG (uveitic, silicone-induced, neovascular, post-keratoplasty, aphakic)	16 (44)	6	1	7	2	0.0639 ^b
Other (congenital, Sturge–Weber syndrome)	4 (11)	0	0	3	1	0.4824 ^b
Previous glaucoma or conjunctival-involving surgery, <i>N</i> (% of eyes)						
Trabeculectomy	7 (19)	0	1	5	1	0.3393 ^b
Ahmed Glaucoma Valve	2 (6)	0	1	1	0	N too small
Pars plana vitrectomy	7 (19)	3	0	3	1	0.2716 ^b
XEN gel stent	1 (3)	0	1	0	0	N too small
Preserflo Microshunt	1 (3)	0	0	1	0	N too small
IOP at baseline, mmHg (m±SD)	28.9±11.3	23±11	27.2±8.4	33.2±12.6	25±9.1	0.1562 ^c
IOP at 12 months, mmHg (m±SD)	14.9±5.1	17±7.1	12.8±2.8	16.5±4.4	11.6±4.0	0.0758 ^c
Topical medications at baseline, <i>N</i> (m±SD)	2.9±1.0	3.3±0.8	3.0±0.0	2.7±1.1	2.9±1.4	0.6342 ^d
Topical medications at 12 months, <i>N</i> (m±SD)	1.0±1.1	1.6±1.3	0.6±0.9	1.3±1.2	0.1±0.5	0.0473 ^d
Absolute success at 12 months, %	46.6	28.6	60	28.6	88	0.0452 ^e
Qualified success at 12 months, %	71.8	57	100	61.4	88	0.2105 ^e
Stent removal, <i>N</i>	3	n/a	2 (month 1)	n/a	1 (month 1)	n/a
Post-operative complications, <i>N</i> (%) ^f						
HypHEMA	7 (19)	1 (14)	0	3 (19)	3 (38)	0.3923 ^b
Shallow AC	2 (6)	0	1 (20)	1 (6)	0	N too small
Hypotony ^g	12 (33)	0	3 (60)	6 (38)	3 (38)	0.1519 ^b
Choroidal effusion	7 (19)	1 (14)	1 (20)	1 (6)	4 (50)	0.0833 ^b

Abbreviations: ACP, Ahmed ClearPath; AGV, Ahmed Glaucoma Valve; BGI, Baerveldt Glaucoma Implant; IOP, intraocular pressure; m±SD, mean±standard deviation; N, number; PACG, primary angle closure glaucoma; PGI, Paul Glaucoma Implant; PK, penetrating keratoplasty; POAG, primary open angle glaucoma; SACG, secondary angle closure glaucoma; SOAG, secondary open angle glaucoma.

^aSome patients had both eyes operated but implanted with different GDD.

^bChi-square test.

^cOne-way ANOVA test.

^dKruskal-Wallis test.

^eManthel-Cox log rank test.

^fSome eyes had more than one complication (i.e. hypHEMA and hypotony). All cases of hypHEMA, shallow AC hypotony or choroidal effusions resolved spontaneously within 1–2 weeks.

^gHypotony was numerically defined by IOP<6mmHg at any timepoint.

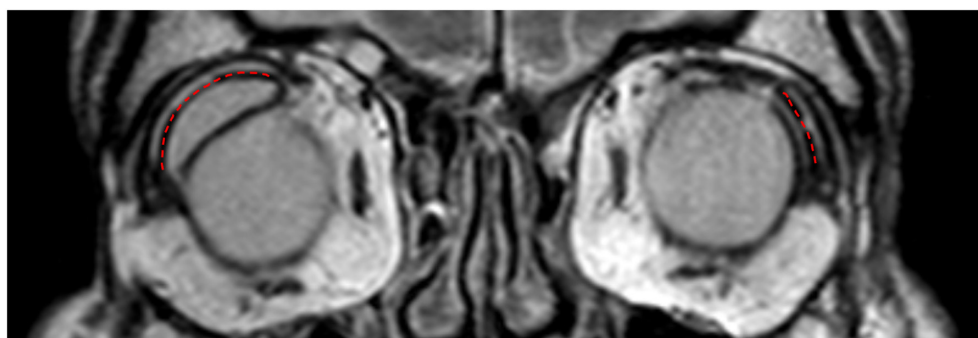


FIGURE 1 T2-weighted coronal scan of a patient implanted with a PGI (right eye) and an AGV (left eye). The dotted red lines represent the hypointense endplate, with the over and underlying hyperintense fluid pockets representing pooled AH (i.e. a double-layered bleb). Flattening of the scleral bed underneath the inferior bleb of the PGI (right eye) is also observed.

3.3 | Surgical success and safety profile

Mean pre-operative IOP was significantly reduced at 12 months (28.9 ± 11.3 vs. 14.9 ± 5.1 mmHg; $p < 0.0001$), as was the number of medications (2.9 ± 1.0 vs. 1.0 ± 1.1 ; $p < 0.0001$). Cumulative probability of unmedicated (absolute) and medicated success (qualified) was 46.6 and 71.8%, respectively. All cases of failure were due to uncontrolled IOP failing to meet success criteria, except one patient with a PGI who underwent surgical revision. Kaplan–Meier survival curves for the overall sample are shown in Figure 3 and clinical and outcome comparisons between groups are detailed in Table 2. All complications were recorded within the first month of surgery and were self-limited, except two cases of hypotony with BGI devices recorded after the first month, immediately following stent removal.

3.4 | Clinical correlations

Total and inferior bleb volumes showed a significant inverse correlation with IOP at day 7 post-operatively ($r_s =$

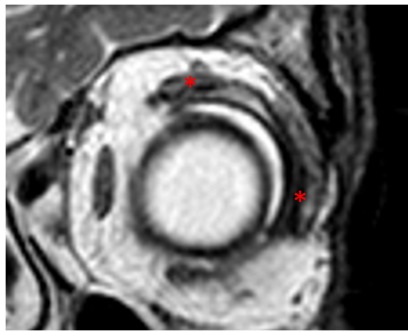


FIGURE 2 T2-weighted coronal scan of an eye implanted with an ACP device showing the double-bleb sign (a thick inferior layer and a thin superior layer) the bleb signal extending both superior and lateral recti muscles (red asterisk).

TABLE 3 Summary of radiological findings and measurements.

	Total	AGV	BGI	PGI	ACP	<i>p</i> -value
Eyes, <i>N</i>	36	7	5	16	8	0.0157 ^a
Time from surgery to MRI (days)	85 ± 66	82 ± 47	46 ± 24	96 ± 83	90 ± 58	0.7052 ^b
Bleb volume, total (mm ³)	563 ± 390	332 ± 190	390 ± 337	734 ± 434	533 ± 346	0.1223 ^b
Bleb volume, inferior (mm ³)	276 ± 202	101 ± 64	199 ± 185	380 ± 205	271 ± 178	0.0108 ^b
Globe volume (mm ³)	5863 ± 1811	6888 ± 1925	5563 ± 2223	4900 ± 861.4	6640 ± 2913	0.3706 ^c
Endplate to limbus (mm)	8.5 ± 1.9	8.6 ± 2.5	10.2 ± 0.8	8.3 ± 2.0	7.1 ± 1.1	0.2301 ^b
Endplate to optic nerve (mm)	9.5 ± 4.0	12.5 ± 5.3	8.7 ± 3.8	8.8 ± 3.3	8.9 ± 3.9	0.2519 ^b
Axial length (mm)	23.5 ± 3.4	24.5 ± 4.4	21.5 ± 2.8	23.4 ± 3.5	24.2 ± 2.8	0.4603 ^b
Bleb extension under recti, <i>N</i> (%)	22 (61)	0 (0)	3 (60)	13 (81)	6 (75)	0.0024 ^a
Double-layered blebs, <i>N</i> (%)	34 (94)	7 (100)	3 (60)	16 (100)	8 (100)	0.0044 ^a
Scleral flattening, <i>N</i> (%)	12 (33)	0 (0)	1 (17)	10 (63)	1 (17)	0.0089 ^a

Note: *p*-value is in reference to comparisons between the 4 GDD subgroups.

Abbreviations: ACP, Ahmed ClearPath; AGV, Ahmed Glaucoma Valve; BGI, Baerveldt Glaucoma Implant; MRI, magnetic resonance imaging; *N*, number of;

PGI, Paul Glaucoma Implant.

^aChi-square test.

^bOne-way ANOVA test.

^cKruskal-Wallis test.

-0.3326 , $p = 0.0475$; $r = -0.3434$, $p = 0.0403$; respectively). Conversely, there was a significant positive correlation between total volume and IOP at 12 months of follow-up ($r_s = 0.3592$, $p = 0.0341$), which was not observed with the inferior bleb ($r_s = 0.2661$, $p = 0.1223$). These correlations are graphically displayed as best-fit lines using linear regression in Figure 4. We observed no other significant correlation between bleb volume and other clinical variables, such as time elapsed from surgery to MRI, age, axial length, globe volume or with IOP at other time-points (data not shown). Moreover, patients with a history of previous glaucoma or conjunctival-involving surgery showed similar total bleb volumetry comparing with surgically naïve patients (543 ± 411 vs. 583 ± 379 mm³, respectively; $p = 0.7658$). Cox regression analysis showed no significant influence of bleb volume on survival probability ($\beta = 0.0009388$; HR = 1.001; $p = 0.1709$).

4 | DISCUSSION

Our results suggest that GDD blebs form around the endplate, translating into a double-layer configuration on imaging scans. The double-layered bleb sign means that the endplate does not stay opposed to the sclera. Since the endplate is anchored to the sclera along its

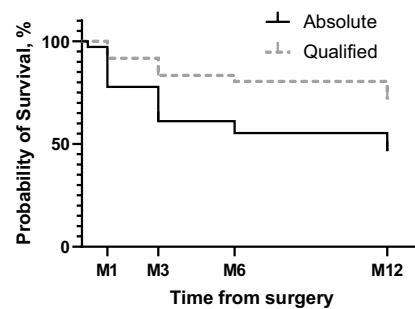


FIGURE 3 Kaplan–Meier survival curves for the overall sample.

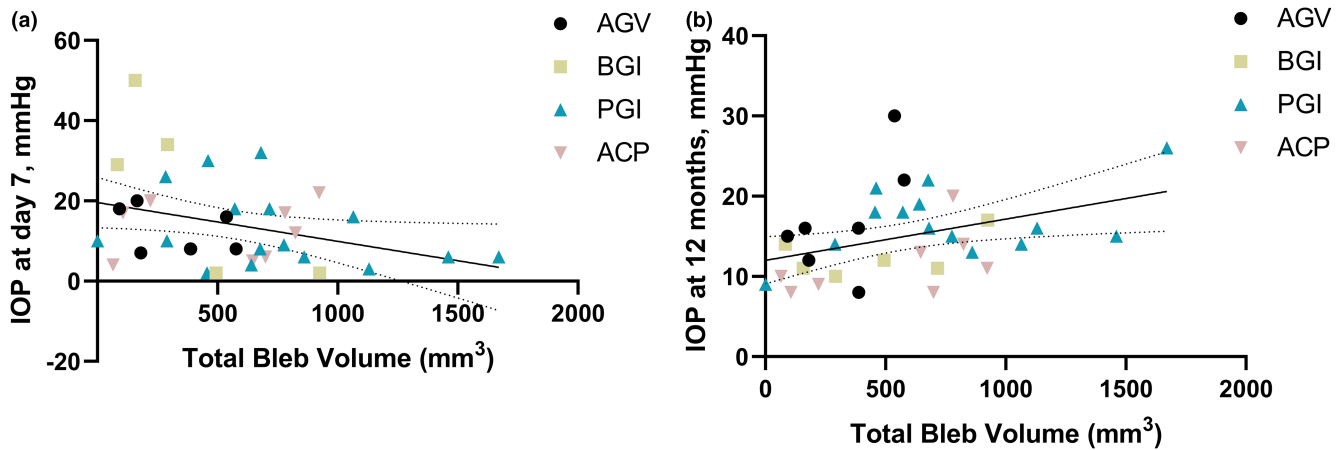


FIGURE 4 Plot and best-fit line of the IOP measurements and total bleb volume. Each point represents an eye. (a) IOP at day 7 and total bleb volume. (b) IOP at month 12.

anterior aspect, as AH pools beneath the plate and raises its posterior aspect, the tube could, in theory, tilt inside the AC, as previously suggested (Ferreira et al., 2015), although studies have shown AGV and BGI tubes usually move closer to the cornea over time (Lopilly Park et al., 2012; Tan et al., 2014). The double-bleb sign has been previously reported with variable frequencies across the literature (Anderson et al., 2017; Ferreira et al., 2015; Sano et al., 2015). Indeed, Iwasaki et al. (2017) found about only half of BGI imaged showed a double-layered bleb but his sample was imaged significantly later (average 15.2 ± 10.1 months), which may indicate that the distribution of aqueous between the upper and lower ‘compartments’ may vary over time. Also, Islamaj et al. (2022) published a series of 7-Tesla MRI scans on BGI patients, which showed double-layered blebs with large inferior blebs (492.3 mm^3 on average) with visible connective tissue strands within the endplate fenestrations, which suggests these strands may have a limited function regarding bleb volume restriction.

We have also shown that despite the measured total bleb volume being similar across the four types of GDD ($p=0.1223$), the total bleb volume observed with the PGI device was significantly higher when compared with the other grouped GDDs (AGV, BGI and ACP; 734 ± 434 vs. $427 \pm 286 \text{ mm}^3$; $p=0.0167$). This difference in volume may be especially attributed to the size of the inferior layer of PGI blebs, which was significantly different across devices ($p=0.0108$). Larger blebs with the PGI may be explained by its different design and the surgical technique. The reduced lumen of the PGI (roughly a third of the inner lumen of BGI and ACP tubes) may offer a higher resistance to flow, according to Poiseuille's law, which is why we did not stent the PGI and but placed an additional ligature around the tube as hypotony prevention. We hypothesize that the absence of an intraluminal stent may offer a lower resistance to early flow compared with stented BGI and ACP devices, which would determine a more aggressive early bleb expansion resulting in overall larger blebs. The larger PGI inferior blebs, which effectively elevate the endplate against the conjunctiva, may theoretically pose an increased risk of erosion or extrusion of the device in the long-term.

Our data also shows that most devices implanted with ‘winged’ endplates extend their blebs along the surface area of the endplate (22/29 eyes with BGI, PGI and ACP, collectively), including into the space under the muscles, which suggests that this space is clinically useful. We also report that larger volume blebs in the 75th–100th quartile were significantly associated with scleral flattening underneath the bleb ($p=0.0049$). This is likely associated with the volume effect and has been reported previously with large BGI blebs (Islamaj et al., 2022).

Previous publications have drawn a wide range of correlations between IOP and bleb morphology at different timepoints. Detorakis et al. (2009) and Sano et al. (2015) reported an inverse correlation between IOP and bleb volume. Conversely, Ferreira et al. (2015) reported an positive correlation between bleb dimensions (height and volume) and pre- and post-operative IOP, while other studies reported no correlations (Islamaj et al., 2022; Iwasaki et al., 2017).

Interestingly, we found opposing correlations between bleb volume and IOP measurements at different timepoints. An inverse correlation between bleb volume and IOP at day 7 and a direct correlation at 12 months were found. This may be due to a higher distensibility of the subconjunctival space in the early post-operative period faced with a higher flow rate, which would account for a significant drop in IOP and enlargement of the bleb within the first week after surgery. Experimental reports have shown higher flow rates in larger blebs versus smaller blebs (Bouremel et al., 2019; Minckler et al., 1987) and Ferreira et al. reported a strong positive correlation between bleb volume and pre-operative IOP in AGV devices imaged at a similar timepoint compared to our series (Ferreira et al., 2015). Conversely, larger blebs may be associated with elevated IOP later in the follow-up due to increased mechanical stress on the bleb capsule wall (owing to the bleb's larger radius, according to Laplace's law), which may thicken in response and increase its resistance to AH absorption (Minckler et al., 1987; Molteno et al., 2003; Wilcox & Kadri, 2007). Anderson et al. (2017) reported an increase in bleb height on consecutive MRI scans from 0–2 weeks up to 4–6 months post-operative on eyes

implanted with a BGI and an early inverse correlation between bleb height and IOP, which later disappeared at the 6 months point supporting the assertion that initial bleb expansion is driven by an increased flow rate with concurrent IOP reduction.

Authors have hypothesized that there may be a risk of longer endplates abutting the optic nerve, causing damage (Kahook et al., 2006). Our data suggests that a standardized implantation technique aiming for a 10 mm distance from the limbus ensures a 'safe' average minimum distance from the endplate to the optic nerve of 9.5 ± 4.0 mm, considering a 2 mm 'safe zone'.

Regarding secondary outcomes, our data shows all GDD were effective in lowering IOP and medication, with a reported an overall absolute and qualified probability of success of 46.6% and 71.8%. Most recorded complications appeared early in the post-operative period and were self-limited, with no serious, sight-threatening complication recorded (Table 2). These results are in line with previously published series, although direct comparison is limited by our smaller sample size and the wide range of success criteria across the literature (Budenz et al., 2015, 2016; Christakis et al., 2016; Dorairaj et al., 2022; Grover et al., 2022; José et al., 2022; Tan et al., 2022; Tsai & Budenz, 2017; Vallabh et al., 2022).

This study has several limitations. First, it consists of a relatively small sample, with significantly more eyes implanted with PGI devices than with other GDDs. Secondly, the time from surgery from MRI varied both within and across GDD subgroups. Further studies will help clear some of the questions raised in our study concerning the clinical value of GDD bleb morphology assessment. The use of higher resolution imaging would be more appropriate in attempting to discern the bleb wall and its thickness.

To our knowledge, this is one of the largest series detailing bleb morphology features of GDDs using MRI. Moreover, it is the first to do so across a wide spectrum of devices, including newly introduced devices such as the PGI and ACP, and the first study of this kind to systematically record the distance between implanted GDD and the optic nerve. We conclude that GDDs overwhelmingly form a double-layered bleb, which should correspond, tridimensionally, to an encircling bleb around the device endplate. We also report that bleb volume may correlate with IOP control dynamically, with early bleb expansion being associated with lower IOP but larger blebs ultimately predicting higher long-term IOP. Furthermore, we posit that an unstented and unvalved GDD such as the PGI produces larger blebs due to higher early outflow. Finally, a standardized 10 mm implantation distance from the limbus seems to ensure a safe distance of the endplate to the optic nerve, regardless of the device.

ACKNOWLEDGEMENTS

Interim results of this project were presented at the 2022 ARVO meeting (May 1–5 2022, Denver, Colorado, USA). Consequently the abstract for this presentation was published: Rafael Correia Barão et al.; Magnetic Resonance Imaging of Glaucoma Drainage Devices. *Invest. Ophthalmol. Vis. Sci.* 2022;63(7):3710 – A0395.


ORCID

Rafael Correia Barão  <https://orcid.org/0000-0002-3102-1969>

David Berhanu  <https://orcid.org/0000-0003-1851-7182>

Diogo Bernardo Matos  <https://orcid.org/0000-0002-6929-4524>

André Diogo Barata  <https://orcid.org/0000-0002-0976-5603>

Rita Sousa  <https://orcid.org/0000-0002-6096-8182>

Luís Abegão Pinto  <https://orcid.org/0000-0002-9960-7579>

REFERENCES

- Anderson, D.M., Schwoppe, R.B., Reiter, M.J. & Suhr, A.W. (2017) Magnetic resonance imaging characteristics of a Baerveldt glaucoma implant. *Journal of Glaucoma*, 26(6), 534–540.
- Barton, K., Gedde, S.J., Budenz, D.L., Feuer, W.J. & Schiffman, J. (2011) The Ahmed Baerveldt comparison study: methodology, baseline patient characteristics, and intraoperative complications. *Ophthalmology*, 118(3), 435–442.
- Bouremel, Y., Lee, R.M.H., Eames, I., Brocchini, S. & Khaw, P.T. (2019) Novel approaches to model effects of subconjunctival blebs on flow pressure to improve clinical grading systems after glaucoma drainage surgery. *PLoS One*, 14(10), 1–15.
- Budenz, D.L., Barton, K., Gedde, S.J., Feuer, W.J., Schiffman, J., Costa, V.P. et al. (2015) Five-year treatment outcomes in the Ahmed Baerveldt comparison study. *Ophthalmology*, 122(2), 308–316.
- Budenz, D.L., Feuer, W.J., Barton, K., Schiffman, J., Costa, V.P., Godfrey, D.G. et al. (2016) Postoperative complications in the Ahmed Baerveldt comparison study during five years of follow-up. *American Journal of Ophthalmology*, 163(3), 75–82.e3.
- Christakis, P.G., Kalenak, J.W., Tsai, J.C., Zurakowski, D., Kammer, J.A., Harasymowycz, P.J. et al. (2016) The Ahmed versus Baerveldt study: five-year treatment outcomes. *Ophthalmology*, 123(10), 2093–2102.
- Conlon, R., Saheb, H. & Ahmed, I.I.K. (2017) Glaucoma treatment trends: a review. *Canadian Journal of Ophthalmology*, 52(1), 114–124.
- Desai, M.A., Gedde, S.J., Feuer, W.J., Shi, W., Chen, P.P. & Parrish, R.K. (2011) Practice preferences for glaucoma surgery: a survey of the American Glaucoma Society in 2008. *Ophthalmic Surgery, Lasers, and Imaging*, 42(3), 202–208.
- Detorakis, E.T., Maris, T., Papadaki, E., Tsilimbaris, M.K., Karantanis, A.H. & Pallikaris, I.G. (2009) Evaluation of the position and function of aqueous drainage implants with magnetic resonance imaging. *Journal of Glaucoma*, 18(6), 453–459.
- Dorairaj, S., Checo, L.A., Wagner, I.V., Hulzen, R.D.T. & Ahuja, A.S. (2022) 24-month outcomes of Ahmed ClearPath® glaucoma drainage device for refractory glaucoma. *Clinical Ophthalmology*, 16(July), 2255–2262.
- Ferreira, J., Fernandes, F., Patricio, M., Brás, A., Rios, C., Stalmans, I. et al. (2015) Magnetic resonance imaging study on blebs morphology of Ahmed valves. *Journal of Current Glaucoma Practice*, 9(1), 1–5.
- Grover, D.S., Kahook, M.Y., Seibold, L.K., Singh, I.P., Ansari, H., Butler, M.R. et al. (2022) Clinical outcomes of Ahmed ClearPath implantation in glaucomatous eyes: a novel Valveless glaucoma drainage device. *Journal of Glaucoma*, 31(5), 335–339.
- Hoffmann, E.M., Herzog, D., Wasieleca-Poslednik, J., Schuster, A.K. & Butsch, C. (2020) Bleb grading by photographs versus bleb grading by slit-lamp examination. *Acta Ophthalmologica*, 98(5), e607–e610.
- Ishida, K., Nakano, Y., Ojino, K., Shimazawa, M., Otsuka, T., Inagaki, S. et al. (2021) Evaluation of bleb characteristics after trabeculectomy and glaucoma implant surgery in the rabbit. *Ophthalmic Research*, 64(1), 68–76.
- Islamaj, E., Van Vught, L., Jordaán-Kuip, C.P., Vermeer, K.A., Ferreira, T.A., De Waard, P.W.T. et al. (2022) Magnetic resonance imaging reveals possible cause of diplopia after Baerveldt glaucoma implantation. *PLoS One*, 17(10 October), 1–13.
- Iwasaki, K., Kanamoto, M., Takihara, Y., Arimura, S., Takamura, Y., Kimura, H. et al. (2017) Evaluation of bleb fluid after Baerveldt glaucoma implantation using magnetic resonance imaging. *Scientific Reports*, 7(1), 1–8.

- José, P., Barão, R.C., Teixeira, F.J., Marques, R.E., Peschiera, R., Barata, A. et al. (2022) One-year efficacy and safety of the PAUL glaucoma implant using a standardized surgical protocol. *Journal of Glaucoma*, 31(3), 201–205.
- Jung, K.I., Park, H., Jung, Y. & Park, C.K. (2015) Serial changes in the bleb wall after glaucoma drainage implant surgery: characteristics during the hypertensive phase. *Acta Ophthalmologica*, 93(4), e248–e253.
- Kahook, M.Y., Noecker, R.J., Pantcheva, M.B. & Schuman, J.S. (2006) Location of glaucoma drainage devices relative to the optic nerve. *British Journal of Ophthalmology*, 90(8), 1010–1013.
- Khamar, M.B., Soni, S.R., Mehta, S.V., Srivastava, S. & Vasavada, V.A. (2014) Morphology of functioning trabeculectomy blebs using anterior segment optical coherence tomography. *Indian Journal of Ophthalmology*, 62(6), 711–714.
- Koh, V., Chew, P., Triolo, G., Lim, K.S., Barton, K., Aquino, C. et al. (2020) Treatment outcomes using the PAUL glaucoma implant to control intraocular pressure in eyes with refractory glaucoma. *Ophthalmology Glaucoma*, 3(5), 350–359.
- Lloyd, M.A., Baerveldt, G., Nguyen, Q.H. & Minckler, D.S. (1996) Long-term histologic studies of the Baerveldt implant in a rabbit model. *Journal of Glaucoma*, 5(5), 334–339.
- Lopilly Park, H.Y., Jung, K.I. & Park, C.K. (2012) Serial intracameral visualization of the Ahmed glaucoma valve tube by anterior segment optical coherence tomography. *Eye (London, England)*, 26(9), 1256–1262.
- Minckler, D.S., Shammass, A., Wilcox, M. & Ogden, T.E. (1987) Experimental studies of aqueous filtration using the Molteno implant. *Transactions of the American Ophthalmological Society*, 85, 368–392.
- Molteno, A.C.B., Fucik, M., Dempster, A.G. & Bevin, T.H. (2003) Otago glaucoma surgery outcome study: factors controlling capsule fibrosis around Molteno implants with histopathological correlation. *Ophthalmology*, 110(11), 2198–2206.
- Oh, L.J., Wong, E., Lam, J. & Clement, C.I. (2017) Comparison of bleb morphology between trabeculectomy and deep sclerectomy using a clinical grading scale and anterior segment optical coherence tomography. *Clinical and Experimental Ophthalmology*, 45(7), 701–707.
- Rathi, S., Andrews, C.A., Greenfield, D.S. & Stein, J.D. (2021) Trends in glaucoma surgeries performed by glaucoma subspecialists versus nonspecialists on Medicare beneficiaries from 2008 through 2016. *Ophthalmology*, 128(1), 30–38.
- Sano, I., Tanito, M., Uchida, K., Katsube, T., Kitagaki, H. & Ohira, A. (2015) Assessment of filtration bleb and endplate positioning using magnetic resonance imaging in eyes implanted with long-tube glaucoma drainage devices. *PLoS One*, 10(12), 1–13.
- Siggel, R., Schroedl, F., Dietlein, T., Koch, K.R., Platzl, C., Kaser-Eichberger, A. et al. (2020) Absence of lymphatic vessels in non-functioning bleb capsules of glaucoma drainage devices. *Histology and Histopathology*, 35(12), 1521–1531.
- Tan, A.N., De Witte, P.M., Webers, C.A., Berendschot, T.T., De Brabander, J., Schouten, J.S. et al. (2014) Baerveldt drainage tube motility in the anterior chamber. *European Journal of Ophthalmology*, 24(3), 364–370.
- Tan, M.C.J., Choy, H.Y.C., Koh Teck Chang, V., Aquino, M.C., Sng, C.C.A., Lim, D.K.A. et al. (2022) Two-year outcomes of the Paul glaucoma implant for treatment of glaucoma. *Journal of Glaucoma*, 31(6), 449–455.
- Tsai, J.C. & Budenz, D.L. (2017) Five-year pooled data analysis of the Ahmed Baerveldt comparison study and the Ahmed versus Baerveldt study. *American Journal of Ophthalmology*, 176, 118–126.
- Vallabh, N.A., Mason, F., Yu, J.T.S., Yau, K., Fenerty, C.H., Mercieca, K. et al. (2022) Surgical technique, perioperative management and early outcome data of the PAUL® glaucoma drainage device. *Eye*, 36(10), 1905–1910.
- Vinod, K., Gedde, S.J., Feuer, W.J., Panarelli, J.F., Chang, T.C., Chen, P.P. et al. (2017) Practice preferences for glaucoma surgery: a survey of the American Glaucoma Society. *Journal of Glaucoma*, 26(8), 687–693.
- Wagdy, F.M. (2020) Bleb morphology using anterior-segment optical coherence tomography after Ahmed glaucoma valve surgery with tenon capsule resection. *Journal of Ophthalmology*, 2020, 8386135.
- Waibel, S., Spoerl, E., Furashova, O., Pillunat, L.E. & Pillunat, K.R. (2019) Bleb morphology after mitomycin-C augmented trabeculectomy: comparison between clinical evaluation and anterior segment optical coherence tomography. *Journal of Glaucoma*, 28(5), 447–451.
- Wilcox, M. & Kadri, O.A. (2007) Force and geometry determine structure and function of glaucoma filtration capsules. *Ophthalmologica*, 221(4), 238–243.
- Yang, S.A., Mitchell, W., Hall, N., Elze, T., Lorch, A.C., Miller, J.W. et al. (2021) Trends and usage patterns of minimally invasive glaucoma surgery in the United States: IRIS® registry analysis 2013–2018. *Ophthalmology Glaucoma*, 4(6), 558–568.
- Yu, D.Y., Morgan, W.H., Sun, X., Su, E.N., Cringle, S.J., Yu, P.K. et al. (2009) The critical role of the conjunctiva in glaucoma filtration surgery. *Progress in Retinal and Eye Research*, 28(5), 303–328.

How to cite this article: Correia Barão, R., Berhanu, D., Bernardo Matos, D., Barata, A.D., Sousa, R. & Abegão Pinto, L. (2023) Bleb morphology of glaucoma drainage devices on magnetic resonance imaging. *Acta Ophthalmologica*, 101, 789–796. Available from: <https://doi.org/10.1111/aos.15668>